Article

Optimized Fuel Economy Control of Power-Split Hybrid Electric Vehicle with Particle Swarm Optimization

Hsiu-Ying Hwang and **Jia-Shiun Chen** *

Department of Vehicle Engineering, National Taipei University of Technology, Taipei 10608, Taiwan; hhwang@mail.ntut.edu.tw
* Correspondence: chenjs@mail.ntut.edu.tw

check for updates

Abstract: This research focused on real-time optimization control to improve the fuel consumption of power-split hybrid electric vehicles. Particle swarm optimization (PSO) was implemented to reduce fuel consumption for real-time optimization control. The engine torque was design-variable to manage the energy distribution of dual energy sources. The AHS II power-split hybrid electric system was used as the powertrain system. The hybrid electric vehicle model was built using Matlab/Simulink. The simulation was performed according to US FTP-75 regulations. The PSO design objective was to minimize the equivalent fuel rate with the driving system still meeting the dynamic performance requirements. Through dynamic vehicle simulation and PSO, the required torque value for the whole drivetrain system and corresponding high-efficiency engine operating point can be found. With that, the two motor/generators (M/Gs) supplemented the rest required torques. The composite fuel economy of the PSO algorithm was 46.8 mpg, which is a 9.4% improvement over the base control model. The PSO control strategy could quickly converge and that feature makes PSO a good fit to be used in real-time control applications.

Keywords: hybrid electric vehicle; power-split; fuel economy; particle swarm optimization

1. Introduction

Since the industrial era, the demand for fossil fuels has increased and the burning of fossil fuels has led to an increase in global carbon dioxide emissions, which has also increased global warming. The National Oceanic and Atmospheric Administration (NOAA) conducted a network sampling of carbon dioxide concentration based on 40 regions around the world. The survey found that since 1979, the global atmospheric carbon dioxide concentration has risen sharply. With a carbon dioxide concentration of 336 ppm in 1979, the global atmospheric carbon dioxide concentration has reached 414 ppm in March 2020. According to Taiwan's CO2 emissions survey by the Environmental Protection Agency of the Ministry of Administration, the energy sector's CO2 emissions accounted for approximately 10.5% of total fuel combustion emissions, industry accounted for 47.8%, transportation accounted for 14.6%, services accounted for 13.4%, residential emissions accounted for 12.6%, and agriculture accounted for 1.1% [1]. It is clear that transportation emissions are the second-largest source, after industrial emissions.

Due to carbon dioxide emissions, major car manufacturers currently commit to the development of new energy to replace gasoline, including electric energy, solar energy, biomass energy, etc. Many automobile manufacturers are optimistic about electric energy since it can be practically used in mass production. With low fuel consumption and exhaust emissions, hybrid electric vehicles (HEVs) have been attracting widespread public attention in recent years. Hendrickson et al. [2] presented the GM

two-mode, front-wheel-drive hybrid powertrain, detailing the mechanical structure and operating mode of this powertrain system. Meisel et al. [3] presented the power distribution of the hybrid transmission in different modes and four fixed-gear ratios in detail. They also compared the differences between the Toyota THS-II gearbox and the GM two-mode gearbox, aiming at energy loss and engine fuel consumption. The advantages of the GM two-mode power system were clearly explained. For the hybrid electric vehicle architecture, the control strategy of the vehicle is critical and is mainly to allocate energy and improve energy efficiency. Many energy management strategies for hybrid electric vehicles have been proposed. They can be divided into two main types: those with 1 a rule-based strategy, and those with 2 an optimization strategy. Torres et al. [4] focused on rule-based controls. The benefits of these controls were rapid rule design and easy implementation. Schouten et al. [5] applied fuzzy logic in HEV control strategies. The rules were judged based on the accelerator and brake pedal signals, battery state of charge (SOC), and motor speed. This optimization method heavily relied on the experience and intuition of the engineers.

The optimization strategy for vehicle fuel economy simulation can be categorized into two areas, global optimization and real-time local optimization. The global optimization algorithm requires completing the whole driving cycle in order to obtain the best fuel economy. This makes it difficult to apply on real road scenarios. Genetic algorithms (GAs) are one of the global optimization algorithms. Montazeri et al. [6] applied GA optimization in parallel HEVs, where the engine torque and battery SOC were design variables with the objective of minimizing fuel consumption and emissions. Dynamic programming (DP) is another typical global optimization algorithm. Wu et al. [7] presented the application of DP on electric buses and used DP to explore energy management strategies for range-extended electric buses (REEBs). Zheng et al. [8] applied stochastic DP in plug-in hybrid vehicles to achieve a global optimization. Wang et al. [9] implemented the DP algorithm in a plug-in HEV (PHEV) and showed a 20% improvement in fuel consumption. DP analyzes the whole driving cycle, searching for minimum fuel consumption to get the global optimum. It provides an improvement for fuel economy; however, it takes a lot of time for the whole simulation and process. An alternative way is to utilize the optimum patterns obtained from pre-calculated DP, such as rule-based (RB) control. RB can be adapted for real-time applications; however, the fuel economy of RB might not be as good as DP's due to the instant change in actual scenarios.

For real-time applications, optimized fuel consumption needs to be carried out quickly for each time step. Local optimization can be suitable for the applications. The equivalent consumption minimization strategy (ECMS) does not require long calculation and is one control algorithm fitting for real-time fuel consumption optimization. Paganelli et al. [10] presented the application of the equivalent consumption minimization strategy (ECMS) in parallel HEVs. They managed the power distribution to minimize fuel consumption, which includes the actual fuel consumed by the engine and an equivalent fuel converted from the electrical energy consumed by motors. Their simulation maintained the battery SOC in a reasonable range by applying a penalty function to ensure battery life. Particle swarm optimization (PSO) is another real-time control algorithm for vehicle fuel consumption. Chen et al. [11] discussed the application of particle swarm optimization (PSO) on HEVs. They optimized the engine output power as an energy management strategy. Wu et al. [12] applied PSO to plug-in HEVs. The main goal of their study was to optimize the control strategy to achieve the best fuel economy. For charge depleting (CD) mode, restrictions were imposed to optimize the PSO. Abido et al. [13] applied PSO to the energy flow control problem of buses. The main goal was to minimize fuel consumption and improve voltage stability. Wang et al. [14] applied a particle-swarm-optimization-based nonlinear model predictive control strategy on a series-parallel hybrid electric bus to optimize the fuel consumption. Chen et al. [15] discussed the application of PSO on plug-in HEVs (PHEVs). In terms of vehicle speed, fuzzy logic judgments were added. Then, the PSO determined the upper and lower limits of the required engine power to obtain the optimal result. Chen et al. [16] implemented improved particle swarm optimization (IPSO) in HEVs. The difference from the original PSO was mainly to add the value of a poor function. This function would cause the

PSO particles to speed-up to find the best solution. Beside ECMS and PSO, there are other control algorithms to achieve better fuel economy. Zheng et al. [17] applied Pontryagin's minimum principle to optimize a parallel plug-in hybrid electric bus. Feng et al. [18] combined an artificial neural network model and a fuzzy-logic controller to optimize the fuel consumption of a hybrid electric mining truck. Comparing the differences between PSO and genetic algorithms (GAs), GAs remove the worst position at one time, and PSO keeps the worst particles, judging the best solution according to the position of each particle [18]. In addition, GAs mainly process the replication, mating, and mutation, which requires a large amount of calculation [19]. Relatively speaking, since the information transmission between PSO particles and the interaction mechanism between particles is relatively simple in PSO, the amount of calculation is lower and the delivery time can be shortened. With the advantages of quick convergence, the PSO algorithm is suitable for real-time control applications for vehicle fuel consumption optimization. This research applied PSO for real-time optimization control.

In 2018, global battery electric vehicle (BEV) and HEV sales exceeded 5.1 million, a significant increase of 63% from the previous year. BEVs and HEVs will become the first choice for the public in the future. The two-mode hybrid (TMH) system was the power system applied in this research. A basic rule-based control was implemented as the base model with an initial energy management strategy, and the simulation result was compared to the manufacturer data. Then, the PSO control strategy was added to optimize fuel consumption and explore the reasons for improvement. This paper investigated a TMH system that had power-split hybrid functionality.

2. Modeling

In this research, a simulation model was created with Matlab/Simulink that included a vehicle, TMH transmission system, internal combustion engine (ICE), motor/generators (M/Gs), battery, and controller, as shown in Figure 1. With the United States FTP-75 (EPA Federal Test Procedure) of urban and highway driving cycles, the vehicle model could estimate the torque and power required for driving. The controller module (Controller) determined the transmission mode switching and the optimal output torques of the engine and M/Gs. The transmission module simulated the torques and speeds of the two motor/generators. The battery module would simulate the battery's state of charge (SOC) and battery charge and discharge status. These modules are presented in the following sections.
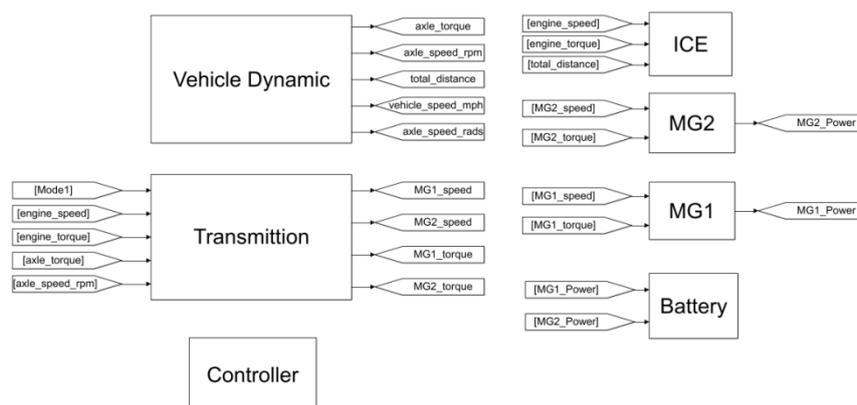
Figure 1. Simulink model of two-mode power-split hybrid system.

2.1. Vehicle Model

U.S. FTP-75 (EPA Federal Test Procedure) was employed in this model. The vehicle model estimated the required driving torque according to the vehicle speed from the driving cycles. The driving resistance forces included aerodynamic resistance, rolling resistance, and grading resistance.

The FTP-75 driving cycles include urban and highway sections. The total distance traveled in the urban cycle is 17.77 km, the total time is 1874 s, the average speed is 34.1 km/h, and the highest speed

is 91.2 km/h, as shown in Figure 2. The total distance of the highway cycle is 16.5 km, the total time is 765 s, the average speed is 77.7 km/h, and the maximum speed is 96.4 km/h, as shown in Figure 3.
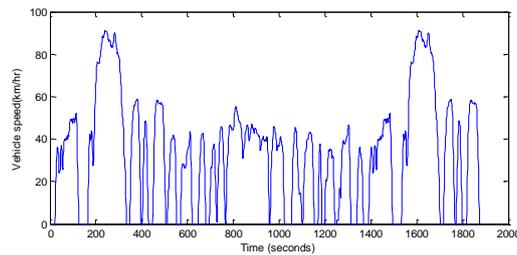
Figure 2. US EPA FTP75 urban driving cycle.
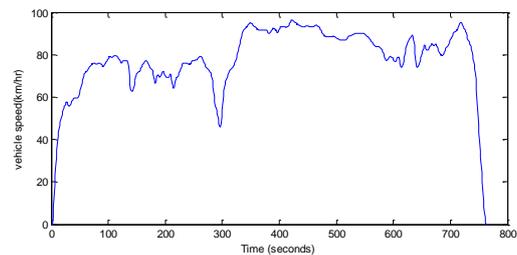
Figure 3. US EPA FTP75 highway driving cycle.

2.2. Transmission Model

In this research, the two-mode hybrid transmission, 2MT70, was implemented as the hybrid electric powertrain system. The entire powertrain was composed of several main components, as shown in Figure 4, which included a simple planetary gear set, a compound planetary gear set, four sets of clutches, two electric motors/generators, an IC engine, and a battery [20].
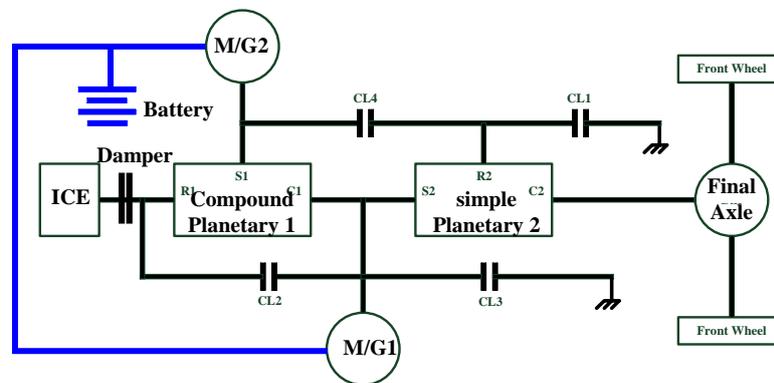
Figure 4. Driveline configuration of two-mode hybrid power system.

2.3. Internal Combustion Engine Model

The internal combustion engine (ICE) module mainly cooperated with the brake-specific fuel consumption (BSFC) lookup table according to the engine speed and torque to find the corresponding fuel rate. The total fuel consumption of the driving cycle was obtained through integration. A V-6 3.6-L engine efficiency chart is shown in Figure 5.
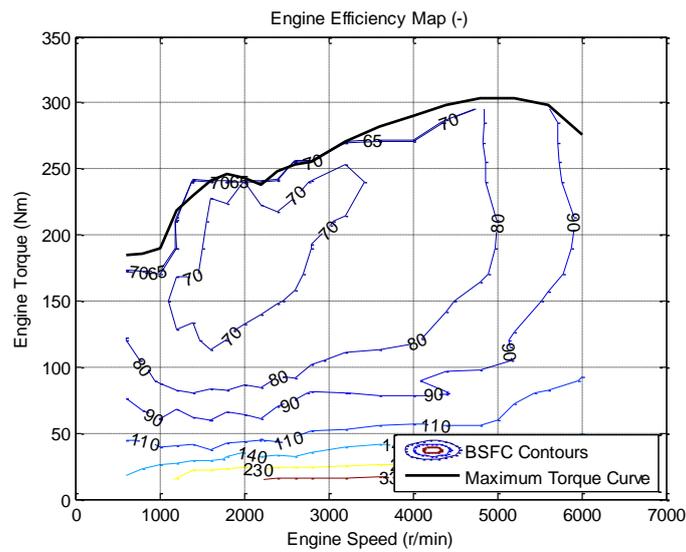
Figure 5. Internal combustion engine's efficiency chart.

2.4. Electric Motor/Generator Model

The electric motor/generator (M/G) modules obtain the operating efficiency of the electric motor through a three-dimensional lookup table based on the current speed and torque. Two 60 kW permanent magnet AC motors were constructed. The efficiency diagram is shown in Figure 6. The power of the M/G was calculated as Equation (1).

$$P_{MG} = \omega_{MG} T_{MG} \eta_{MG}^k \tag{1}$$

P_{MG}, ω_{MG}, and T_{MG} are the power, speed, and torque of the electric motor/generator, respectively. η_{MG} represented the efficiency of M/G. If the values of the torque and the speed were positive or negative at the same time, the M/G was consuming power and performing as an electric motor. If the values of the speed and torque were of the opposite sign, the M/G was charging and running as a generator. k represents the energy path. If M/G operated as an electric motor, k was −1. If it operated as a generator, k was +1.
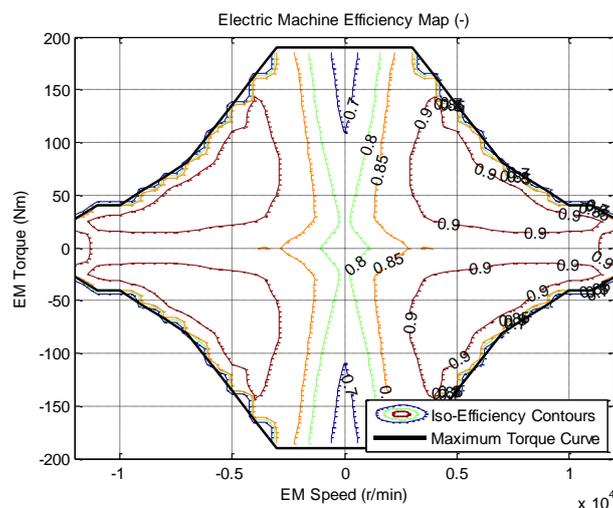
Figure 6. Motor/generator's efficiency chart.

2.5. Battery Model

The electric power required by the M/Gs was provided by the battery, and the total power of the battery was estimated through the motor's power and efficiency, as presented in Equation (2).

$$P_{batt} = T_{MG1}\omega_{MG1}\eta_{MG1}^k\eta_{c1}^k + T_{MG2}\omega_{MG2}\eta_{MG2}^k\eta_{c2}^k \tag{2}$$

P_{batt} is the power of the battery, η_c is the efficiency of the electric converter, T_{MG} is the M/G torque, ω_{MG} is the speed of the M/G, η_{MG} is the efficiency of the M/G, and k indicates the energy path. $k = -1$ indicates that the battery was discharged, and $k = 1$ indicates that the battery was charged.

The battery module was composed as an equivalent circuit, including open circuit voltage and a battery pack, as shown in Figure 7. I_{batt} represents the battery current, and P_{batt} is the battery output or input power.
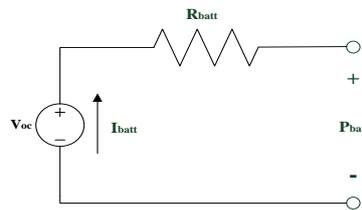
Figure 7. Diagram of battery equivalent circuit.

The relationship between battery SOC and current I_{batt} is as follows.

$$\dot{SOC} = -\frac{I_{batt}}{Q_{\max}} \tag{3}$$

Q_{max} is the ampere-hour capacity of the battery at the current rate I_{batt}. The battery current, open circuit voltage, and internal resistance would vary according to the battery power. The relationship between battery output or input power and current is presented as follows.

$$P_{batt} = V_{OC}I_{batt} - I_{batt}^2 R_{batt} \tag{4}$$

$$I_{batt} = -\frac{V_{OC} - \sqrt{V_{OC}^2 - 4P_{batt}R_{batt}}}{2R_{batt}} \tag{5}$$

$$\dot{SOC} = -\frac{V_{OC} - \sqrt{V_{OC}^2 - 4\left(T_{MG1}\omega_{MG1}\eta_{MG1}^k\eta_{c1}^k + T_{MG2}\omega_{MG2}\eta_{MG2}^k\eta_{c2}^k\right)R_{batt}}}{2R_{batt}Q_{\max}} \tag{6}$$

where V_{oc} is the battery open circuit voltage and R_{batt} is the battery's internal resistance.

2.6. Controller Model

2.6.1. Rule-Based Controller

The controller module had three main functions: the first one was the control of switching mode, which decided the timing of switching between the first and the second mode according to the driving cycle; the second one was based on the driving condition and battery SOC to determine the controlled engine speed and engine torque according to the rules established in the controller; the third one was engine state control logic. To achieve fuel saving, the engine would be turned off when it was not required to provide driving power.

2.6.2. PSO Controller

This controller module also had three main functions: the first one was to decide the time of switching, which was the same as the rule-based controller; the second one was to determine the engine speed, which was based on the drive resistance and battery SOC, and the engine torque, which was estimated by the particle swarm algorithm; the third one was the engine state control, which was determined by the PSO controller. The only exception was if the vehicle traveled at very low speed and the engine was turned off—then the rule-based control was used.

3. Energy Management Optimization

3.1. Particle Swarm Algorithm

Particle swarm optimization (PSO) is a group-based optimization search method [21,22]. The advantage is that it has a fast convergence speed and fewer parameter settings. The swarm movement of birds was simulated. Birds usually maintain a specific formation when they travel as a group, and individuals will maintain a certain distance from each other. The search technology of PSO is mainly to simulate the social behavior of birds foraging. When birds are searching for food, individuals will understand the relationship between themselves and food. At the same time, the closest individual to food in the flock is also observed. So, when searching for food, the best path can be found based on these two points. Assume that food is considered as the global best solution in the function and the distance between each individual in the flock and the food is used as the objective degree of the function. Then, the process of each individual in the flock seeking food can be the process to search for the optimized solution. This concept is the foundational idea of the PSO algorithm.

The detailed calculation steps of the PSO algorithm are as follows: x_i^t and v_i^t are defined as the position and flight speed of the *i*-th particle in the particle group at time *t*, respectively. The model of the PSO algorithm can be divided into speed update function and position update function as follows.

The main process steps of PSO are:

1. Initialize the position and velocity of each particle using random numbers.
2. Use the objective function to calculate the objective value for each particle.
3. Compare the current objective value with the best position of the particle, P_{best}. If the currently searched objective value is better than P_{best}, the new objective value and position will be applied to update the value of P_{best}.
4. Compare the currently searched objective value with the best value in the group, g_{best}. If the currently searched value is better than g_{best}, use the new value and position of the particle to update g_{best}.
5. Change the speed and position of the particles according to Equations (7) and (8).

$$v_i^t = \omega * v_i^{t-1} + c_1 * rand() * \left(p_i - x_i^{t-1}\right) + c_2 * rand() * \left(g_i - x_i^{t-1}\right) \tag{7}$$

$$x_i^t = x_i^{t-1} + v_i^t \tag{8}$$

where x_i^t is the position of the *i*-th particle at time t, v_i^t is the speed of the *i*-th particle at time *t*, p_i is the best position that the *i*-th particle has traveled to, g_i is the best position that all particles have traveled to, c_1 is the weight of one's own experience to make particles closer to the best solution of the individual, c_2 is the weight of the group's experience to make the particles closer to the best solution of the group, ω is the inertia weight, which affects the range and speed of convergence, and *rand()* is a random value used to maintain the diversity of group movement directions.

3.2. PSO Algorithm Applied to Hybrid Electric Power System

This research implemented PSO to find the minimum instantaneous fuel consumption at each driving moment. The process of the PSO algorithm is described as follows.

1. Initialization: This research applied engine torque as the initial particle position. The initial flying speed was randomly generated. To avoid exceeding the operational range of engine torque during the algorithm search process, the constrained equations were included in the simulation. The engine torque constrained condition is shown in Equation (9). Since the PSO algorithm did not have a practical mechanism to control the speed of the particles, the constrained condition was set for the speed Equation (10). During the particle search process, the battery SOC must be ensured to avoid over-charging and over-discharging. The constrained equation for the SOC upper and lower limits is shown in Equation (11).

$$T_{E,\min} < T_E < T_{E,\max} \tag{9}$$

$$v_{i,\min}^t < v_i^t < v_{i,\max}^t \tag{10}$$

$$SOC_{i,\min}^t < SOC_i^t < SOC_{i,\max}^t \tag{11}$$

where T_E is the engine torque, v_i is the particle speed, and SOC_i^t is the battery state of charge at time t, $T_{E,min}$ is the lower limit of engine torque, $T_{E,max}$ is the upper limit of engine torque, $v_{i,min}$ is the lower limit of particle speed, $v_{i,max}$ is the upper limit of particle speed, $SOC_{i,min}^t$ is the lower limit of the SOC, and $SOC_{i,max}^t$ is the upper limit of the SOC.

2. Apply the objective function: In order to improve the performance of the system, a suitable objective function was designed to allow particles to search for the objective value. The lowest instantaneous equivalent fuel consumption was the best solution of this optimization problem. So, instantaneous equivalent fuel consumption was applied as the objective function as in Equation (12).

$$F_{obj} = \dot{m}_{eq} + \beta = \dot{m}_e(T_E, \omega_E) + W(SOC)\dot{m}_b + \beta \tag{12}$$

where $\dot{m}_{eq}$ is the sum of the instantaneous equivalent fuel consumption, $\dot{m}_e(T_E, \omega_E)$ is the instantaneous fuel consumption of the engine, $\dot{m}_b$ is the equivalent fuel consumption of the battery's electrical energy, β is a penalty value to avoid the particle searching process violating restrictions, and *W(SOC)* is the weight factor to prevent the power of the battery from being depleted.

The instantaneous fuel consumption of electric power was calculated by Equation (13). The battery power consumption was converted to the equivalent fuel consumption, $\dot{m}_b$, by the engine BSFC corresponding to the engine torque and speed.

$$\dot{m}_b = \frac{\left(\zeta_{discharge} * \overline{BSFC} * \frac{P_{MG}}{\eta_{batt}*\eta_{MG}} + \zeta_{charge} * \overline{BSFC} * P_{MG} * \eta_{batt} * \eta_{MG}\right)}{1000 * 3600} \tag{13}$$

where $\dot{m}_b$ is the conversion of battery power consumption into equivalent fuel consumption, $\overline{BSFC}$ is the BSFC corresponding to engine torque and speed, P_{MG} is the electric motor power, η_{batt} is the battery operating efficiency, η_{batt} is the electric motor working efficiency. $\zeta_{discharge}$ is the battery discharge factor, and ζ_{charge} is the battery charge factor.

3. Select and memorize: Each particle would remember the corresponding objective value and compare it with the value obtained by the particle at the previous moment. After determining the best value, P_{best}, of each particle, the values of all particles were compared to determine the best value in the group, g_{best}. With the best value, g_{best}, of the group, the corresponding engines best torque could be received.

4. Modify particle's speed and position: Each particle's T_E was moved to the next position according to Equations (7) and (8).

5. End rule: Set the convergence conditions. If the convergence conditions were not met, steps 2–4 until the particle search met the convergence conditions.

3.3. Formulation of PSO Algorithm

3.3.1. Initialization and Parameter Setting

Initially, four particles were generated randomly. In this research, vehicle performance was improved by optimizing the instantaneous fuel consumption and the engine torque was applied as the particle's position. The particles' initial position and speed were assigned as follows.

$$\begin{bmatrix} x_1^t & x_2^t & x_3^t & x_4^t \end{bmatrix} = \begin{bmatrix} T_{E,1}^t & T_{E,2}^t & T_{E,3}^t & T_{E,4}^t \end{bmatrix} = \begin{bmatrix} 0 & 10 & 20 & 30 \end{bmatrix} \tag{14}$$

$$\begin{bmatrix} v_1^t & v_2^t & v_3^t & v_4^t \end{bmatrix} = \begin{bmatrix} -1 & -2 & 2 & 4 \end{bmatrix} \tag{15}$$

The lower speed limit, $v_{i,\min}^t$, and upper speed limit, $v_{i,\max}^t$, were set between (–10–10). If the value of the speed vector was too large, it would cause the particles to jump out of the area with a good solution. If the value of the speed vector was too small, it would cause the particles to fall into the local minimum value. For the better solution, the particle speed was usually set to 10–20% of the search range [18]. The learning factors were both set as 2.

3.3.2. Evaluate Each Particle

The objective value of each particles position was measured. In the initial state, random particles were first moved by the random speed and the updated position of the particles was compared with the initial random position to obtain the local optimal position, P_{best}. Then, based on their own experience and group experience among the particles, the particles moved to the new positions. To avoid unreasonable particle positions and over-charge or over-discharge of the battery, some constraints were set as follows.

$$0 < T_E < 220 \tag{16}$$

$$0.4 < SOC < 0.6 \tag{17}$$

3.3.3. Evaluate the End of Searching

If the position distances between the particles were less than 0.01, the search result was converged (Equations (18)–(21)) and the optimal solution was reached. To prevent the searching time from being too long, an extra setting was added. If the particle search time was greater than 0.5 s, the current best value was directly taken as the optimal torque of the engine.

$$\left| T_{E,1} - T_{E,2} \right| < 0.01 \tag{18}$$

$$\left| T_{E,2} - T_{E,3} \right| < 0.01 \tag{19}$$

$$\left| T_{E,3} - T_{E,4} \right| < 0.01 \tag{20}$$

$$\left| T_{E,4} - T_{E,1} \right| < 0.01 \tag{21}$$

4. Simulation Results and Discussion

4.1. Vehicle Parameters

The model for this research was implemented with Matlab/Simulink. The parameters of the vehicle are shown in Table 1. A V6 3.6 L engine was applied in this research. This engine had a manufacturer configuration for a midsize power-split HEV, and it was compatible with the power of M/Gs applied in this vehicle. The power-split HEV was designed with this engine in order to maintain the performance as the original ICE version. The additional M/Gs provided the HEV with better acceleration and gradeability.

Table 1. Vehicle parameters.

Engine	
Engine Type	V6, SI
Displacement	3.6 (L)
Peak torque	300 Nm
Peak speed	6000 rpm
EM characteristics	
Type	Permanent magnet motor
Maximum power	60 kW
Maximum speed	10,000 rpm
Peak efficiency	0.92
Peak torque	190 Nm
Battery	
Type	Lithium–ion
Capacity	1.5 kWh
Vehicle characteristics	
Vehicle mass	1600 kg
Radius of tire	0.352 m
Vehicle front area	2642 m^2
Rolling resistance coef.	0.01
Aerodynamic drag coef.	0.386

4.2. Charge and Discharge

In this research, the working range of the battery's SOC was set between 0.4 and 0.6, which could effectively extend the battery's service life. At the same time, the battery's internal resistance was low in this working range, regardless of the state of charge or discharge, as shown in Figures 8 and 9.
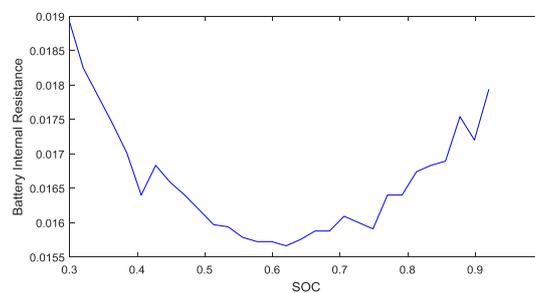
Figure 8. Relation between battery state of charge (SOC) and internal resistance during battery discharge.
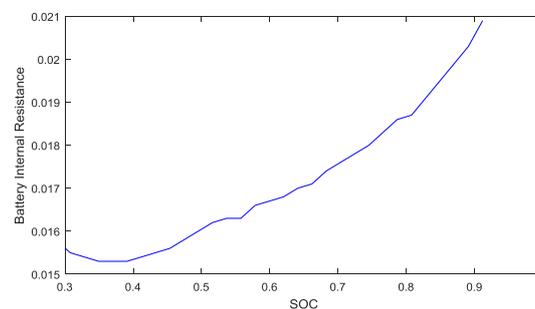
Figure 9. Relation between battery SOC and internal resistance during battery charge.

4.3. Simulation Results

EPA FTP-75 driving cycles were applied in the simulation. The urban and highway driving curves are shown in Figures 2 and 3, respectively. Rule-based simulation results are shown in Table 2. The fuel economy (FE) of urban and highway simulations were 46.28 mpg and 39.11 mpg, respectively,

and the composite FE was 42.74 mpg. The formula for composite FE is shown in Equation (22) As shown in Table 2, the difference between the composite FE of the rule-based simulation and that of the manufacturer data was 0.9%, which was within the allowable range. Therefore, the rule-based control model was applied as a base model to evaluate the optimization simulation of the PSO algorithm.

$$Composite\ FE = \frac{1}{\frac{0.55}{CIty\ FE} + \frac{0.45}{Highway\ FE}} \tag{22}$$

Table 2. Vehicle parameters.

Item	Urban	Highway	Composite
Rule-based	46.28 mpg	39.11 mpg	42.74 mpg
Manufacturer	48 mpg	37 mpg	42.34 mpg

Rule-based control and PSO simulation results are presented in Table 3. In the urban driving cycle, the FE of the rule-based simulation was 46.28 mpg, and the FE of the PSO simulation was 51.79 mpg. PSO showed a 12% improvement over rule-based control. In the highway driving cycle, the FE of the rule-based simulation was 39.11 mpg, and the FE of the PSO simulation was 41.85 mpg. PSO showed a 7% improvement over rule-based control. For composite FE, rule-based control was 42.74 mpg and PSO was 46.78 mpg. PSO showed an improvement of 9.4% compared to rule-based control.

Table 3. Comparison of fuel economy.

	Urban	Highway	Composite
Rule-based	46.28 mpg	39.11 mpg	42.74 mpg
PSO	51.79 mpg	41.85 mpg	46.78 mpg
Improved	12%	7%	9.4%

To understand the reasons for the improvements with the PSO algorithm, the instantaneous fuel consumption of the rule-based control and PSO models were compared, as shown in Figures 10 and 11. Figure 10 shows the urban simulation results; the instantaneous fuel consumption of the PSO was generally smaller than that of the rule-based controller. The switching timing for the engine to turn on/off depended on the required engine torque and battery SOC. In rule-based control, the results were obtained from the pre-set rules/tables. In PSO, the algorithm searched for better fuel consumption under the desired engine torque. Therefore, the fuel rate of PSO was smaller and engine-switch timing was different from rule-based control. Figure 11 shows the instantaneous fuel consumption for the highway driving cycle. It can be seen that the maximum instantaneous fuel consumption was 2.6 g/s for rule-based control and 2.3 g/s for PSO. PSO would affect the engine switch timing and engine operating points. The fuel consumption of PSO was better than that of the rule-based control.
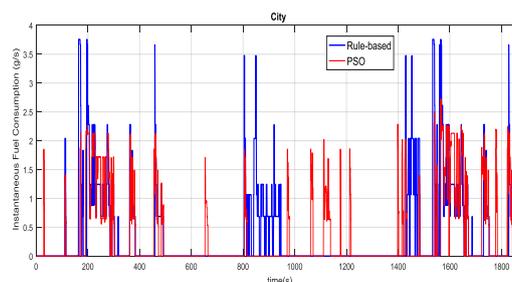
Figure 10. Comparison of instantaneous fuel consumption in the urban driving cycle.
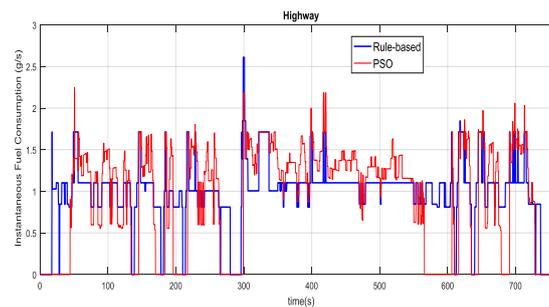
Figure 11. Comparison of instantaneous fuel consumption in the highway driving cycle.

Figures 12 and 13 are comparisons of engine speeds on urban and highway driving cycles, respectively. The engine speeds of PSO and rule-based control were mainly determined by driving resistance and SOC. According to the simulation results of the two methods, most of the engine speeds in urban areas were around 1400 to 2000 rpm. The improvement in fuel consumption was affected by engine torque.
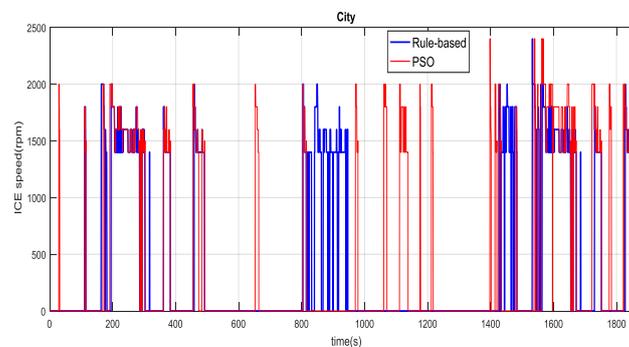
Figure 12. Comparison of engine speed in the urban driving cycle.
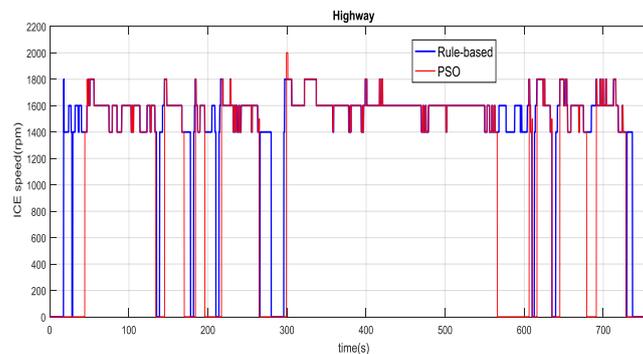
Figure 13. Comparison of engine speed in the highway driving cycle.

Figures 14 and 15 are comparisons of engine torque in urban and highway driving cycles, respectively. It can be seen that the engine torque in PSO was less than that in rule-based control. The peak torque values in urban driving cycles decreased from 250 Nm in rule-based control to 160 Nm in PSO. The reason that PSO algorithm provided a better fuel consumption is mainly due to the engine torque being reduced. In the highway driving cycle, the improvement of fuel consumption was because of different engine operating points and engine running time.
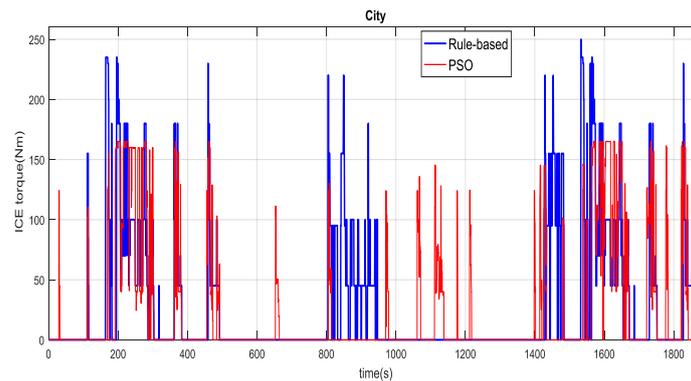
Figure 14. Comparison of engine torque in the urban driving cycle.
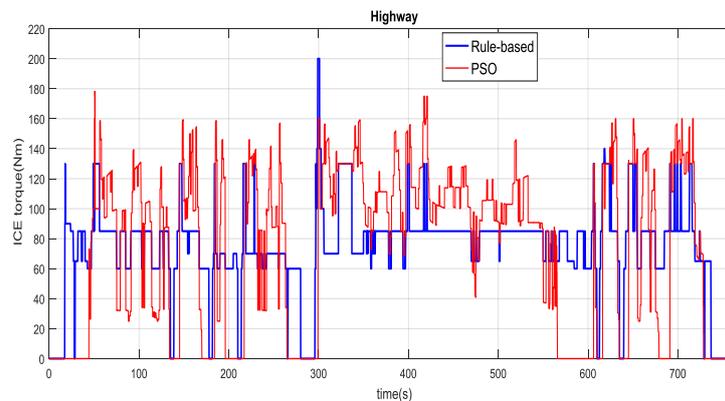
Figure 15. Comparison of engine torque in the highway driving cycle.

Figures 16 and 17 provide the electric conversion loss from the motor/generator to charge the battery. It can be clearly seen that the conversion loss was higher with rule-based control in both driving cycles, which was one of the reasons that PSO could improve the fuel consumption.
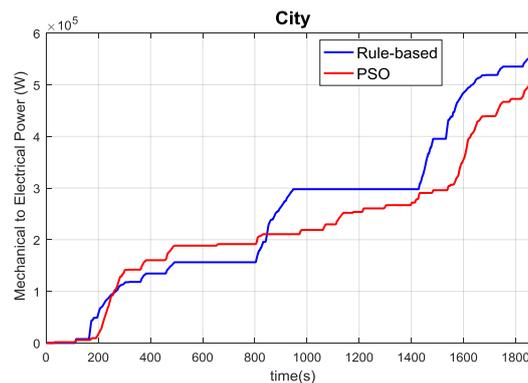
Figure 16. Comparison of electric conversion loss in the urban driving cycle.

Figures 18 and 19 show the engine operating points of rule-based control and PSO in urban areas and the highway driving cycle, respectively. In the urban driving cycle, the engine torque of PSO operating points was mainly in the 50–170 Nm range. Compared to the operating points of rule-based control, the trend of overall PSO engine power decline also led to an improvement of fuel consumption. In rule-based control, some of the engine operating points were around 170–240 Nm, which is in a high-efficiency range. It did not require such a large amount of engine power to drive the vehicle, so the excess engine power would be transferred to the generator to charge the battery. That resulted in an increase of conversion loss. Furthermore, the stored energy in the battery would not stay in the

battery very long and would soon be used for driving. This resulted in a second conversion loss and would affect the fuel economy.
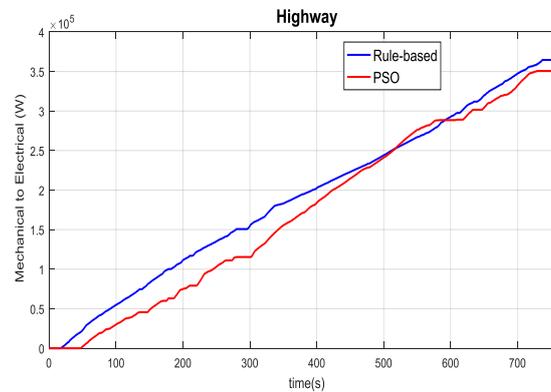
Figure 17. Comparison of electric conversion loss in the highway driving cycle.
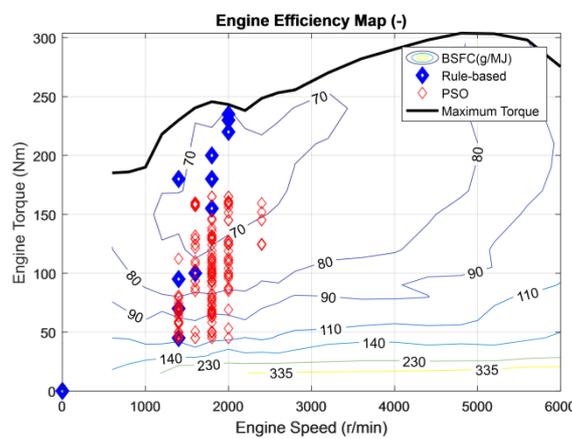
Figure 18. Comparison of urban engine operating points.
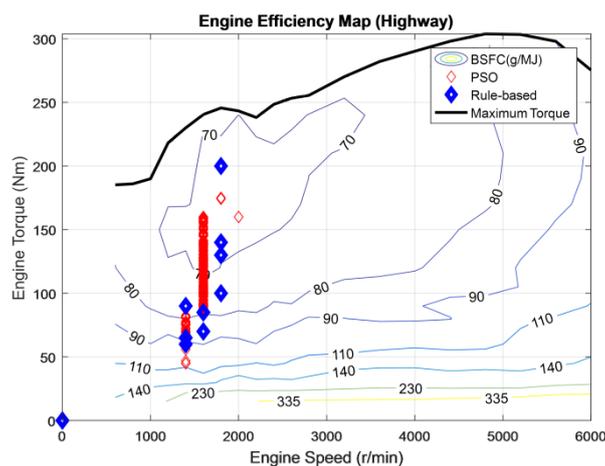
Figure 19. Comparison of highway engine operating points.

On the highway driving cycle, most of the PSO engine operating points were in the range of 75–120 Nm, which is in a better efficiency range of the engine. The engine operating points of rule-based control were scattered throughout a wider range. Some points were around 200 Nm, which is in a high-efficiency region; however, the vehicle did not require such a large amount of engine power. The excess engine power would charge the battery and cause an electric conversion loss. The stored energy

in the battery would be applied for driving. This resulted in a second conversion loss. It affected the fuel economy.

Figures 20 and 21 show the comparison of electric motor torque of M/G1 in urban and highway driving cycles, respectively. M/G1 was mainly driven by the engine in mode one. In the urban driving cycle, M/G1 was mostly in the charge condition. In the highway driving cycle, the powertrain mainly stayed on mode two. M/G1 worked as a driving motor and provided power to drive the vehicle.
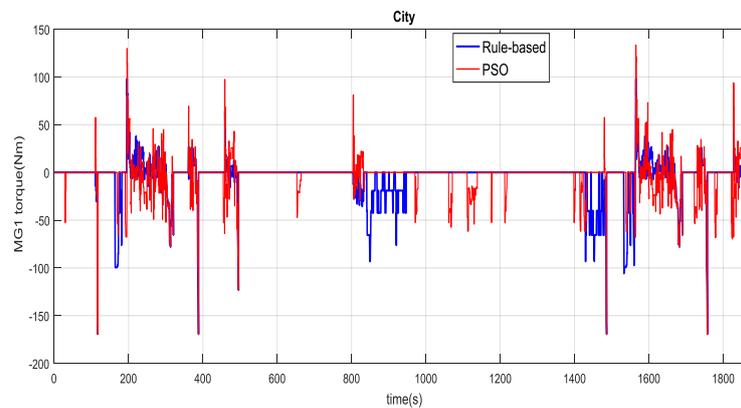
Figure 20. M/G1 torque in the urban driving cycle.
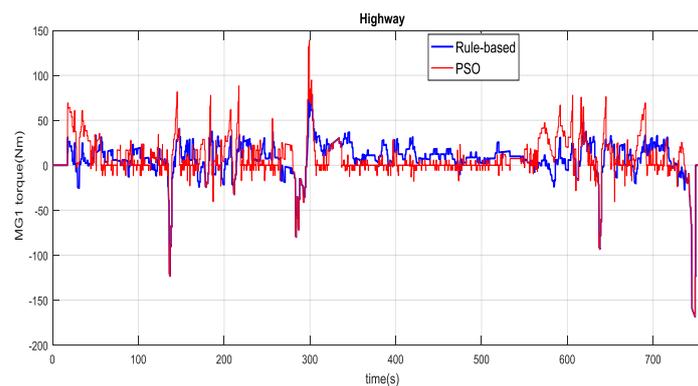
Figure 21. M/G1 torque in the highway driving cycle.

Figures 22 and 23 were the torque of M/G2 in the urban and highway driving cycles, respectively. In the urban driving cycle, the positive torque output time of the PSO algorithm was longer than that of the rule-based control. With the optimization process of the PSO, the vehicle would have more time driven by electric motors to save fuel and improve vehicle fuel economy.
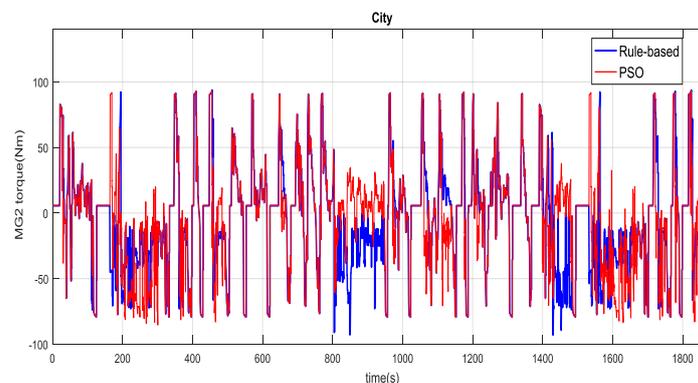
Figure 22. M/G2 torque in the urban driving cycle.
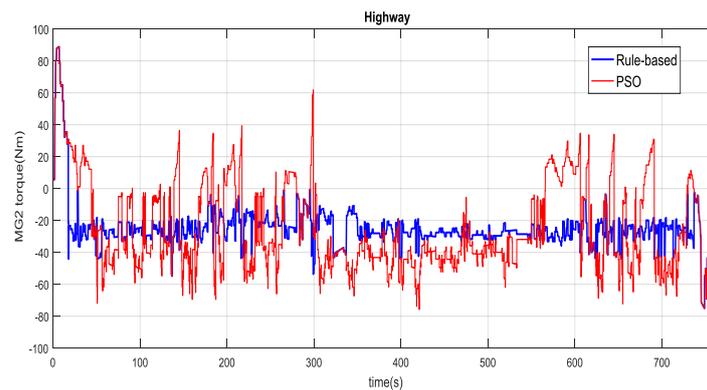
Figure 23. M/G2 torque in the highway driving cycle.

The battery SOC in urban and highway driving cycles are shown in Figures 24 and 25, respectively. Through the driving cycles, the initial SOC and the SOC at the end of the cycles remained very close. During the driving cycle the battery was charged and discharged, and the battery energy at the end of the cycle remained at the same level as at the beginning. All of the driving energy was provided by the engine.
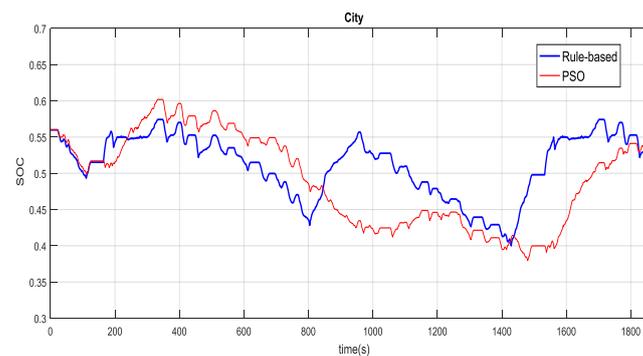
Figure 24. Battery SOC in the urban driving cycle.
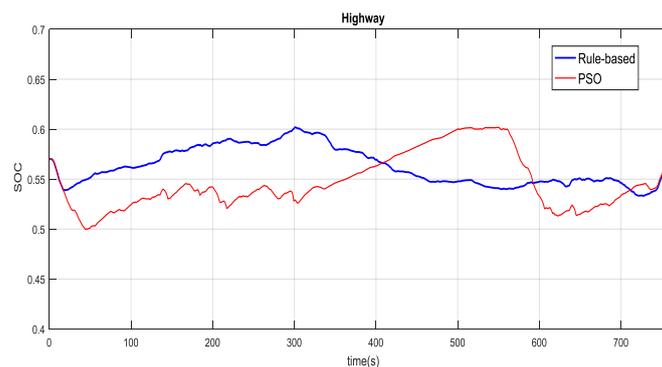
Figure 25. Battery SOC in the highway driving cycle.

5. Conclusions

This research focused on the real-time control algorithm to improve the fuel economy of a two-mode, power-split hybrid electric vehicle. The vehicle model was built with Matlab/Simulink. The fuel economy simulation results of the base model with rule-based control were close to the fuel economy data provided by the original manufacturer, which confirmed the reliability of the vehicle model. Particle swarm optimization (PSO) was implemented as a real-time optimization control with the goal of reducing fuel consumption. The minimum instantaneous fuel consumption was the

objective of PSO. The engine torque was the design variable. PSO was to set up a group of sprinkled particles to search for the best solution. The particles were dispersed in a reasonable working area of the engine, and the value of the objective function was calculated for each particle position. The objective function of each particle and the instantaneous fuel consumption was compared, and the particle position was updated based on better results of the group. The above action was repeated until the particles converged, and the objective value of the particle was the current minimum instantaneous fuel consumption. The following conclusions were obtained based on the simulation results.

1. Urban cycle fuel economy: The result of rule-based simulation was 46.28 mpg; the result of PSO simulation was 51.79 mpg; PSO showed a 12% improvement over rule-based control.
2. Highway cycle fuel economy: The result of rule-based simulation was 39.11 mpg; the result of PSO simulation was 41.85 mpg; PSO showed a 7% improvement over rule-based control.
3. Composite fuel economy: The result of rule-based simulation was 42.74 mpg; the result of PSO simulation was 46.78 mpg; PSO showed an improvement of 9.4% compared to rule-based control.
4. Compared with the rule-based control, PSO could more effectively control the engine on/off switch timing and the engine operating points. With the lower engine torque selected by the PSO algorithm, the engine power and fuel consumption were reduced. With less charging and discharging of the battery, the energy conversion loss was smaller with the PSO algorithm and the vehicle would spend more time driven by electric motors to save fuel and improve vehicle fuel economy.
5. The rule-based control requires long-term accumulated experience to set the rule table. Compared with rule-based control, PSO could find the minimum instantaneous fuel consumption at each moment, achieve real-time control, and improve the fuel economy of power-split HEVs.

Conflicts of Interest: The authors declare no conflict of interest.

References

1. Available online: http://www.epa.gov.tw/ct.asp?xItem=10052&ctNode=31352&mp=epa (accessed on 30 April 2018).
2. Hendrickson, J.; Holmes, A.; Freiman, D. *General Motors Front Wheel Drive Two-Mode Hybrid Transmission*; SAE technical paper 2009-01-0508; SAE World Congress & Exhibition: Detroit, MI, USA, 2009.
3. Meisel, J. *An Analytic Foundation for the Two-Mode Hybrid-Electric Powertrain with a Comparison to the Single-Mode Toyota Prius THS-II Powertrain*; SAE technical paper 2009-01-1321; SAE World Congress & Exhibition: Detroit, MI, USA, 2009.
4. Torres, J.L.; Gonzalez, R.; Gimenez, A.; Lopez, J. Energy management strategy for plug-in hybrid electric vehicles. A comparative study. *Appl. Energy* **2014**, *113*, 816–824. [CrossRef]
5. Schouten, N.J.; Salman, M.A.; Kheir, N.A. Energy management strategies for parallel hybrid vehicles using fuzzy logic. *Control Eng. Pract.* **2003**, *11*, 171–177. [CrossRef]
6. Montazeri-Gh, M.; Poursamad, A.; Ghalichi, B. Application of genetic algorithm for optimization of control strategy in parallel hybrid electric vehicles. *J. Frankl. Inst.* **2006**, *343*, 420–435. [CrossRef]
7. Wu, X.; Chen, J.; Hu, C. Dynamic Programming-Based Energy Management System for Range-Extended Electric Bus. *Math. Probl. Eng.* **2015**, *2015*, 1–11. [CrossRef]
8. Zhang, H.; Qin, Y.; Li, X.; Liu, X.; Yan, J. Power management optimization in plug-in hybrid electric vehicles subject to uncertain driving cycles. *eTransportation* **2020**, *3*, 100029. [CrossRef]
9. Wang, X.; He, H.; Sun, F.; Zhang, J. Application Study on the Dynamic Programming Algorithm for Energy Management of Plug-in Hybrid Electric Vehicles. *Energies* **2015**, *8*, 3225–3244. [CrossRef]

10. Paganelli, G.; Delprat, S.; Guerra, T.M.; Rimaux, J.; Santin, J.J. Equivalent Consumption Minimization Strategy for Parallel Hybrid Powertrains. In Proceedings of the IEEE 55th Vehicular Technology Conference, Birmingham, AL, USA, 6–9 May 2002; pp. 2076–2081.

11. Chen, Z.; Xiong, R.; Wang, K.; Jiao, B. Optimal Energy Management Strategy of a Plug-in Hybrid Electric Vehicle Based on a Particle Swarm Optimization Algorithm. *Energies* **2015**, *8*, 3661–3678. [CrossRef]

12. Wu, X.; Cao, B.; Wen, J.; Bian, Y. Particle Swarm Optimization for Plug-in Hybrid Electric Vehicle Control Strategy Parameter. In Proceedings of the 2008 IEEE Vehicle Power and Propulsion Conference, Harbin, China, 3–5 September 2008; pp. 1–5.

13. Abido, M.A. Optimal power flow using particle swarm optimization. *Int. J. Electr. Power Energy Syst.* **2002**, *24*, 563–571. [CrossRef]

14. Wang, Y.; Wang, X.; Sun, Y.; You, S. Model predictive control strategy for energy optimization of series-parallel hybrid electric vehicle. *J. Clean. Prod.* **2018**, *199*, 348–358. [CrossRef]

15. Chen, Z.; Xiong, R.; Cao, J. Particle swarm optimization-based optimal power management of plug-in hybrid electric vehicles considering uncertain driving conditions. *Energy* **2016**, *96*, 197–208. [CrossRef]

16. Chen, S.-Y.; Hung, Y.-H.; Wu, C.-H.; Huang, S.-T. Optimal energy management of a hybrid electric powertrain system using improved particle swarm optimization. *Appl. Energy* **2015**, *160*, 132–145. [CrossRef]

17. Zhang, S.; Hu, X.; Xie, S.; Song, Z.; Hu, L.; Hou, C. Adaptively coordinated optimization of battery aging and energy management in plug-in hybrid electric bus. *Appl. Energy* **2019**, *256*, 113891. [CrossRef]

18. Feng, Y.; Dong, Z. Optimal energy management with balanced fuel economy and battery life for large hybrid electric mining truck. *J. Power Sources* **2020**, *454*, 227948. [CrossRef]

19. Kennedy, J.; Eberhart, R. Particle Swarm Optimization. In Proceedings of the ICNN'95-International Conference on Neural Networks (ICNN), Perth, WA, Australia, 27 November–1 December 1995; pp. 1942–1948.

20. Hwang, H.-Y.; Lan, T.-S.; Chen, J.-S. Optimization and Application for Hydraulic Electric Hybrid Vehicle. *Energies* **2020**, *13*, 322. [CrossRef]

21. Eberhart, R.; Kennedy, J. A New Optimizer Using Particle Swarm Theory. In Proceedings of the Sixth International Symposium on Micro Machine and Human Science Micro Machine and Human Science, Nagoya, Japan, 4–6 October 1995; pp. 39–43.

22. Eberhart, R.C.; Shi, Y. Comparison between Genetic Algorithms and Particle Swarm Optimization. In *Evolutionary Programming VII-7th International Conference 1998*; Springer: Berlin/Heidelberg, Germany, 1998; Volume 1447, pp. 611–616.